20th IMEKO TC10 Conference
"Measurement for Diagnostics, Optimization and Control to Support Competitiveness and Innovation"
Lisbon, Portugal, September 28–29, 2026

Point Cloud-Based and Multi-Source Data Fusion for Monitoring the State of Conservation of the Defensive Walls of the Historic Town of Mértola, Portugal

Sara Pires[1], Maria João Henriques[2], Dora Roque[2], Hugo Silva[2]

[1]LNEC - National Laboratory for Civil Engineering, Lisbon, Portugal, spires@lnec.pt
[2]LNEC - National Laboratory for Civil Engineering, Lisbon, Portugal

***Abstract* – This paper presents a multi-source point cloud fusion methodology for the three-dimensional documentation and conservation state monitoring of the defensive walls of the Historic Town of Mértola, Portugal. Two Terrestrial Laser Scanner (TLS) campaigns conducted with a 5-month interval were compared to detect and map structural displacements along a critical wall section. A partial wall collapse recorded in the winter of 2025 was documented through a UAV photographic survey of the area. The resulting point cloud was then compared with the post-repair TLS dataset to quantify the volume of lost material, demonstrating the value of point-cloud methods for assessing damage in historic masonry. Geometrically complete point cloud representations of two wall sections were generated by integrating TLS, UAV photogrammetry and 360º spherical imagery, overcoming the geometric limitations of each individual technique. Additionally, a controlled metrological experiment using a test object of known geometry is presented to characterise the influence of scanner viewing angle and range on point cloud quality, providing a quantitative basis for interpreting displacement measurements in complex survey configurations and demonstrating direct implications for the detectability of small-scale surface anomalies relevant to masonry damage assessment.**

Keywords* – *Terrestrial Laser Scanning, UAV photogrammetry, Point cloud fusion, Heritage monitoring, Masonry walls, Sustainable Cities and Communities

I. INTRODUCTION

This paper presents the application of a multi-source point cloud fusion methodology to the defensive walls of the Town of Mértola (Fig. 1), a town of recognised cultural heritage significance, undergoing active conservation assessment. In March 2025, a partial collapse occurred in the Clock Tower-Market (CTM) wall section, resulting in a visible cavity that was subsequently documented through a UAV/drone-based photographic survey to visualize the CTM wall status. Since overlapping photographs were taken of the cavity area, it was possible to perform photogrammetric processing and reconstruct the cavity's geometry, and estimate the volume of lost material before restoration. This event highlights the critical role of systematic point cloud-based monitoring for the detection and quantification of damage in vulnerable masonry structures, particularly when such localised failures may remain unrecorded prior to repair interventions.

Fig. 1 Overview of Town of Mértola.

Two sections of the wall were considered for analysis: the CTM and the Western Wall (WW), located near Mértola Castle. For the CTM section, two terrestrial laser scanning (TLS) campaigns, conducted in September 2025 and February 2026, were co-registered to enable the assessment of structural displacements. Additionally, the March 2025 UAV dataset of the cavity area was integrated with the September 2025 TLS data of the surrounding wall to reconstruct the pre-repair point cloud representation of the affected area.

To ensure geometrically complete representations, multi-source point cloud datasets combining TLS and UAV photogrammetry were generated. For the WW, 360º spherical imagery was additionally incorporated to the TLS and UAV data. These integrated models support a more comprehensive structural assessment and provide a robust basis for heritage documentation.

Furthermore, a controlled experimental study was conducted in a multi-storey building, independent of the surveyed heritage structures, to evaluate the influence of laser scanning range, incidence angle and scanner setup regularity on point cloud quality, providing insight into the geometry-related limitations observed in the field data.

II. RELATED RESULTS IN THE LITERATURE

In surveying, point clouds are typically generated from two types of data acquisition: range-based methods, such as TLS and image-based methods, relying on photographs acquired from aerial (UAV) or terrestrial (standard or 360º) cameras. Range-based methods obtain 3D coordinates directly, by measuring the time-of-flight or phase-shift of a laser pulse emitted toward the surveyed surface and reflected back to the sensor; each measured point is combined with the instrument's known position and orientation to produce a georeferenced 3D coordinate. Image-based methods, by contrast, do not measure distance directly. Instead, 3D geometry is reconstructed computationally from a set of overlapping photographs using Structure from Motion (SfM) and dense multi-view stereo algorithms, which identify common features across images to estimate camera positions and triangulate the corresponding 3D point coordinates. While TLS generally provides higher geometric accuracy and point density for accessible surfaces, image-based methods offer greater flexibility for documenting elevated or otherwise inaccessible areas. Consequently, the complementary use of TLS, UAV photogrammetry and terrestrial imagery has become an increasingly adopted strategy for comprehensive heritage documentation.

The use of point cloud technologies for heritage monitoring has grown substantially over the past decade, particularly in the context of deformation analysis and preventive conservation. Lercari (2019) demonstrated the potential of multi-temporal TLS surveys combined with the Multiscale Model-to-Model Cloud Comparison (M3C2) algorithm to quantify material loss in earthen archaeological structures over extended periods, establishing a replicable workflow aligned with conservation monitoring frameworks [1]. The M3C2 algorithm itself, originally introduced by Lague et al. (2013), provides a robust method for direct comparison of point clouds, particularly suited for rough and complex surfaces typical of heritage structures [2].

Similarly, Sánchez-Aparicio et al. (2024) evaluated 3D imaging techniques for structural assessment of masonry retaining walls, showing that point cloud comparison methods such as Cloud-to-Cloud (C2C) and M3C2 can provide objective and accurate alternatives to traditional visual inspection [3]. The detection and quantification of specific pathologies in historic masonry, such as bulging and deformation, have also been addressed using geometric analysis of point clouds. Hu et al. (2023) proposed a plane-fitting method applied to TLS data to identify deformation areas in ancient city walls, demonstrating the effectiveness of model-based approaches for extracting structural anomalies [4].

The complementarity between TLS and UAV-based photogrammetry is widely recognized in heritage documentation workflow. Fazio et al. (2023) demonstrated that TLS provides high-accuracy data for vertical façades, while UAV photogrammetry effectively captures upper and inaccessible areas, enabling more complete 3D reconstructions [5]. A similar integration strategy was presented by Tsioukas et al. (2024), who employed co-registration techniques within CloudCompare (point cloud processing software) to combine TLS and UAV-SfM datasets for heritage modelling and visualization [6]. In the context of historic fortifications, Moyano et al. further demonstrated the integration of TLS, UAV photogrammetry, and terrestrial imaging into HBIM environments for the Almohad Wall of Cáceres, addressing accessibility constraints comparable to those encountered in Mértola [7].

The integration of heterogeneous point clouds acquired from different sensing technologies has become a key aspect of multi-source heritage documentation. Combining TLS and UAV photogrammetry improves the geometric completeness of 3D models by exploiting the complementary strengths of both techniques, although accurate co-registration remains essential to ensure geometric consistency. Jung et al. (2024) proposed coarse-to-fine Iterative Closest Point (ICP) strategies to improve the alignment of point clouds with different densities and acquisition geometries [8]. The foundations of ICP-based registration methods were established by Besl and McKay (1992), whose work remains fundamental to point cloud registration and alignment [9].

Despite these advances, the influence of acquisition geometry on point cloud quality, particularly in TLS surveys, remains an important but less frequently quantified aspect. Factors such as incidence angle, distance to target and surface orientation and materials can significantly affect point density, noise and measurement accuracy. To address this gap, the present study will include a controlled experimental assessment of TLS data acquired at varying incidence angles and distances, enabling the evaluation of their impact on geometric quality. This experimental component will provide a metrological perspective to interpret observed variations in data quality within the Mértola case study, where steep topographic differences and long acquisition distances introduce non-uniform scanning conditions.

III. DESCRIPTION OF THE METHOD

The proposed methodology integrates multi-temporal TLS, UAV photogrammetry, and 360º spherical imagery to support deformation analysis, multi-source point cloud fusion, and heritage documentation. The approach is structured into several components addressing measurement, fusion and metrological characterisation.

A. Multi-temporal TLS Co-registration and Displacement Detection

Two TLS campaigns were acquired in September 2025 and February 2026 using multiple scan positions to ensure complete façade coverage. Each campaign was independently registered into a unified point cloud using GNSS-RTK referenced Ground Control Points (GCPs), ensuring a consistent geodetic framework [10].

Inter-epoch co-registration was performed in CloudCompare using a hierarchical alignment strategy combining manual pre-alignment and Iterative Closest Point (ICP) optimisation over stable façade regions assumed invariant over time [11]. This step is necessary due to the uncertainty of some centimetres of the GNSS-RTK. Registration quality was assessed through RMSE computed over the selected reference areas, providing an empirical estimate of residual misalignment.

Surface displacement was quantified using the C2C distance computation implemented in CloudCompare. This approach determines the nearest-neighbour distance between point clouds, providing a direct measure of geometric differences between epochs [11]. Although more sensitive to point density variations and surface roughness than normal-based methods, it enables a straightforward assessment of surface changes over the analysed façade [2].

The 2025 dataset was used as the reference cloud for distance computation. A statistical detection threshold was defined based on the combined effects of registration uncertainty and local surface variability, ensuring that only differences exceeding the expected measurement noise were interpreted as potential deformation [12].

B. Cavity Documentation and Volumetric Assessment

A UAV photographic survey was conducted following the partial collapse event of March 2025. This collapse led to rehabilitation interventions made during the Summer of 2025. Image acquisition combined oblique viewpoints to ensure complete geometric coverage of the cavity interior and to minimise occlusions. The images were processed to generate a dense point cloud of the cavity.

The UAV-derived point cloud was registered to the TLS dataset acquired in September 2025, which represents the repaired wall. The cavity reconstructed from the UAV survey was then incorporated into the TLS model by replacing the repaired portion of the wall within the affected area, enabling reconstruction of the pre-repair wall geometry.

The volume of material loss was estimated using the 2.5D Volume tool in CloudCompare. The computation was performed between the TLS point cloud representing the repaired wall and the reconstructed pre-repair model containing the UAV-derived cavity, yielding the volume corresponding to the collapsed material [13].

C. Multi-source Point Cloud Fusion

Multi-source point cloud fusion was performed by integrating TLS, UAV photogrammetry and 360º spherical imagery (the latter used only for the WW section), producing geometrically complete representations of the CTM and WW wall sections.

Data fusion was performed within a unified GNSS-referenced geodetic framework using common GCPs. This multi-sensor integration enables consistent modelling of façade geometry, upper architectural features and surrounding terrain, supporting both structural and heritage documentation [14].

D. Metrological Characterisation of Viewing Geometry Effects

The CTM wall presents challenging acquisition conditions due to its height and the limited locations available for scanner placement, requiring TLS surveys to be performed from relatively long distances and under oblique viewing angles. To investigate the influence of these acquisition conditions on point cloud quality and the reliability of deformation measurements, a controlled experiment was conducted in a multi-storey building using a rigid polystyrene artefact combining a planar and a cylindrical surface, deployed sequentially at two floors offering markedly different acquisition geometries. An upper level - 28 m height (10^{th} floor), surveyed with the TLS at 24 m from the building, reproducing the acquisition conditions of a certain part of the CTM wall, and a lower level - 12 m height (4^{th} floor), surveyed at 13 m from the building, reproducing the shorten acquisition distances encountered at the other part of the CTM wall. The same Leica RTC360 LT scanner used in the field surveys was employed throughout the experiment.

The artefact was surveyed over two independent field sessions. During the first field session, three surveys were acquired: i) one survey at the upper level using a straight-line configuration, parallel to the building, with three scanner setups spaced 7 m apart; ii) a second survey with the same configuration but with the TLS deliberately tilted in one of the setups to isolate the effect of scanner inclination on fitting quality; and iii) a single survey of the lower level, acquired under the same straight-line, 7 m-spaced configuration. During the second field session, two additional surveys were performed at each level: i) one repeating the straight-line, 7 m-spaced configuration, and ii) a second in which setup positions were neither aligned nor regularly spaced, replicating typical uncontrolled field conditions. This design yielded seven independent acquisitions in total, allowing analyse the influence of range, incidence geometry, and setup regularity.

For each of the resulting seven acquisitions, the planar and cylindrical surfaces of the artefact were independently fitted using least-squares plane fitting and nonlinear cylinder fitting (Python, *pye57/scipy*), yielding the fitted equation parameters (plane normal and offset; cylinder axis position, radius) and residual statistics (RMSE, mean, standard deviation, extrema, and the proportion of points exceeding 5 mm and 10 mm deviation thresholds) for both surface types.

To further assess the practical relevance of these findings for masonry surface characterisation, the artefact's planar surface was additionally modified with a set of physical artificial cavities, approximately 10-30 mm in width and 5-10 mm in depth, intended to emulate the type of small-scale surface irregularities observed on the Mértola defensive walls. The analysis of this modified surface was performed using only the data from the second field session.

For each level, the straight-line and uncontrolled-configuration point clouds were co-registered with each other in CloudCompare and converted into a Digital Surface Model (DSM) raster. Rasters were then imported into QGIS and differenced independently at each level, comparing the straight-line vs. uncontrolled acquisitions on both levels, to isolate the effect of scanner setup position and regularity, independently of acquisition range, on the visibility of surface height differences and cavity detail.

IV. RESULTS AND DISCUSSIONS

A. Wall Displacement Monitoring at Mértola

The comparison between the two TLS campaigns of the CTM wall section revealed C2C displacement values predominantly in the maximum range of approximately 1 to 1.5 cm, being the majority towards the interior of the wall. These values are consistent across most of the analysed wall, with no spatially coherent deformation patterns observed.

Considering the uncertainty associated with the GNSS-RTK referenced registration (approximately 3-5 cm), together with the residual uncertainty introduced during point cloud co-registration, the observed displacement magnitudes fall within the expected uncertainty envelope of the measurement system. Consequently, no significant structural changes can be confidently identified, whereas larger or spatially coherent displacements exceeding this uncertainty would be expected to indicate genuine structural deformation.

The UAV-derived point cloud of the collapse cavity was registered to the post-repair TLS dataset to reconstruct the pre-repair geometry of the affected wall section (Fig. 2). The reconstructed and post-repair point clouds were subsequently compared using the 2.5D Volume tool in CloudCompare, yielding an estimated material loss volume of approximately 1.91 m³ and providing a direct quantitative measure of the damage associated with the collapse event.

(a) (b)

Fig. 2 (a) TLS model of the CTM wall section following the Summer 2025 repair intervention; (b) reconstructed pre-repair geometry obtained by incorporating the UAV-derived cavity into the TLS model.

The multi-source fusion of TLS, UAV and spherical imagery produced geometrically complete point cloud representations of both the CTM (Fig. 3) and WW (Fig. 4) wall sections. TLS provided the primary geometric representation of the vertical masonry surfaces, while UAV photogrammetry complemented the dataset by capturing upper and otherwise inaccessible surfaces. For the WW section, 360º spherical imagery further complemented the reconstruction in areas where vegetation and terrain constraints prevented suitable TLS stationing and limited UAV coverage. The integration of these complementary datasets significantly improved the spatial completeness of the final models, particularly in occluded areas.

Fig. 3 Multi-source point cloud representation of the CTM section, integrating TLS and UAV photogrammetry.

Fig. 4 Multi-source point cloud representation of the WW section obtained by integrating TLS, UAV photogrammetry and 360° spherical imagery.

B. Metrological Characterisation Experiment

The controlled metrological experiment conducted in a multi-storey building confirmed a clear, geometry-dependent asymmetry between the two surface types. For each of the seven acquisitions, planar fitting proved highly robust to acquisition geometry: the residual RMSE of the fitted plane, reflecting the deviation of the point cloud from its own best-fit plane, remained within a narrow 0.8–1.5 mm range regardless of floor, scanner alignment, or spacing regularity. Cylinder fitting, by contrast, was more sensitive to acquisition geometry, though this sensitivity was itself range-dependent: at the lower level, RMSE values remained consistently low (1.7-1.9 mm) regardless of whether a straight-line or uncontrolled setup configuration was used, whereas at the upper level, RMSE values remained similarly low (1.9-2.6 mm) under the straight-line configurations but rose markedly to 4.7 mm under the uncontrolled configuration. This suggests that irregular scanner placement degrades cylinder-fitting quality primarily when compounded by the additional noise associated with longer range and steeper incidence angles, rather than acting as an independent source of error. For the survey with a deliberately tilted scanner setup, the resulting fit quality (RMSE 1.9 mm) was statistically indistinguishable from its non-tilted counterpart (2.3 mm), suggesting that moderate deviations in individual setup orientation, on their own, are not a dominant source of noise relative to overall setup spacing and regularity. Notably, the fitted cylinder diameter remained stable (0.690-0.701 m) across all acquisitions regardless of acquisition strategy or level, indicating that geometric bias in the fitted parameter itself is negligible even where local noise is elevated.

Consistent with the above, point density also varied systematically with acquisition geometry: the upper level, acquired at a longer slant range (~38 m) and more oblique incidence (~50°), yielded 5,700-11,000 points per surface, compared to 20,000-30,000 points at the lower level (~18 m range, ~39° incidence). These results establish a quantitative, geometry-controlled noise envelope for interpreting the field displacement values reported in Section IV.E.

The surface-difference analysis performed in QGIS, comparing the straight-line and uncontrolled acquisitions independently at each level, revealed markedly different error distributions between the surveys (Fig. 5). At the upper level, the difference of the surfaces displayed a comparatively uniform pattern, with a larger share of the surface confined within a moderate ±5 mm band and centred on a small systematic offset of approximately 1-2 cm. At the lower level, most of the surface remained very close to zero deviation, while localised discrepancies produced a wider overall range (35.7 mm) and a more heterogeneous, patch-like error distribution.

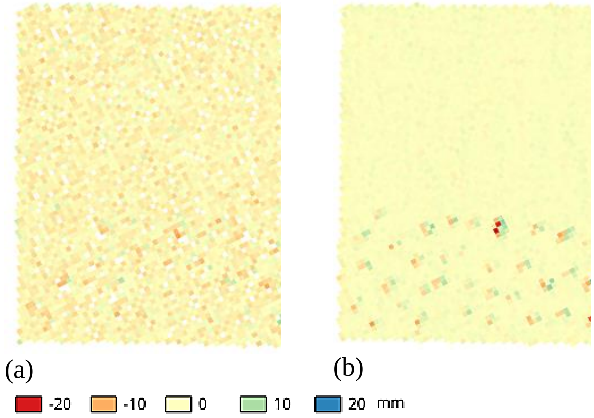

Fig. 5 Surface-difference rasters (QGIS) comparing the straight-line and uncontrolled scanner configurations, computed over the full planar surface of the artefact: (a) upper level; (b) lower level.

This distinction became considerably clearer once the flat, defect-free half of the artefact was examined separately from the half bearing the artificial cavities. Over the flat half alone, the lower level difference surface was visually and statistically far more precise (standard deviation 0.5 mm, range 4.4 mm) than its upper level counterpart (standard deviation 1.3 mm, range 9.5 mm), an image-based confirmation, independent of the plane- and cylinder-fitting residuals reported above, of the density- and range-dependent precision limits associated with acquisition geometry. Over the cavity-bearing half, however, this gap narrowed considerably, with both levels exhibiting comparable variability (standard deviations of 1.8 mm at both levels) and near-identical extreme values, closely reproducing the extrema observed over the full surface. This suggests that, once a genuine surface feature is present, its physical signal dominates over the acquisition-geometry-driven noise that otherwise clearly distinguishes the two floors in the defect-free region.

V. CONCLUSIONS AND OUTLOOK

This work presents a multi-sensor methodology for the geometric analysis and documentation of historic wall structures, combining multi-temporal TLS, UAV photogrammetry, 360º spherical images and multi-source data integration. The application of the C2C algorithm enabled the detection of surface changes between survey epochs, with observed variations remaining within the expected uncertainty range of the measurement system, indicating no significant structural deformation.

The integration of UAV-derived data with TLS proved effective for the reconstruction and volumetric assessment of collapse features, while multi-source point cloud fusion improved the spatial completeness of the resulting point clouds.

The controlled metrological experiment provided a quantitative, geometry-controlled basis for interpreting these field results. Plane fitting proved consistently robust across all tested acquisition geometries, while cylinder fitting, and, more directly, the detectability of small-scale surface irregularities, was shown to degrade with increasing range and incidence angle, and with irregular scanner placement, particularly when these effects compound one another. These findings support the interpretation that the displacement magnitudes observed at the CTM wall section fall within the combined measurement and geometric uncertainty envelope of the survey system, rather than reflecting genuine structural change.

Ongoing work includes the completion of the visual and quantitative documentation of the surface-difference analysis performed on the artefact's cavity-bearing surface, and its incorporation into a broader, range- and geometry-aware uncertainty model for interpreting future TLS-based deformation monitoring at the CTM and WW sections. Continued monitoring of the Mértola defensive walls, informed by this metrological characterisation, will support a more rigorous distinction between measurement noise and genuine conservation-relevant structural change in future survey epochs.

VI. ACKNOWLEDGMENTS

The authors gratefully acknowledge the support of the ATRIUM project (European Union under Grant Agreement No. 101132163), the ARTEMIS project (European Union under Grant Agreement No. 101188009), the ID4CH project (LISBOA2030-FEDER-01317300) and the Municipality of Mértola. The authors also gratefully acknowledge Carlos Serra for providing the equipment used in the metrological experiment.

REFERENCES

[1] **Lercari, N.**: *Monitoring earthen archaeological heritage using multi-temporal terrestrial laser scanning and surface change detection*, Journal of Cultural Heritage, No. 37, 2019, pp. 166–177.

[2] **Lague, D.; Brodu, N.; Leroux, J.**: *Accurate 3D comparison of complex topography with terrestrial laser scanner: Application to the Rangitikei canyon (N-Z)*, ISPRS Journal of Photogrammetry and Remote Sensing, Vol. 82, 2013, pp. 10–26.

[3] **Sánchez-Aparicio, L.J. et al.**: *Experimental evaluation of 3D imaging technologies for structural assessment of masonry retaining walls*, Results in Engineering, Vol. 21, 2024.

[4] **Hu, Y. et al.**: *A study on the detection of bulging disease in ancient city walls based on fitted initial outer planes from 3D point cloud data*, npj Heritage Science, Vol. 11, 2023.

[5] **Fazio, L. et al.**: *Combination of terrestrial laser scanning and UAV photogrammetry for 3D modelling and degradation assessment of heritage building*, npj Heritage Science, 2023.

[6] **Tsioukas, V. et al.**: *Using TLS, UAV, and MR methodologies for 3D modelling and historical recreation of religious heritage monuments*, Journal on Computing and Cultural Heritage, 2024.

[7] **Moyano, J. et al.**: *Integration of SfM, TLS and UAV techniques for HBIM of the Almohad Wall of Cáceres*, ISPRS Archives, 2018.

[8] **Jung, J. et al.**: *Multi-source point cloud registration for urban areas using a coarse-to-fine approach*, GIScience & Remote Sensing, 2024.

[9] **Besl, P.J.; McKay, N.D.**: *A method for registration of 3-D shapes*, IEEE Transactions on Pattern Analysis and Machine Intelligence, Vol. 14, No. 2, 1992, pp. 239–256.

[10] **Girardeau-Montaut, D.**: *CloudCompare - distance computation tools*, 2016. Available: https://www.cloudcompare.org/doc/wiki/index.php/Distances_Computation

[11] **Wheaton, J.M.; Brasington, J.; Darby, S.E.; Sear, D.A.**: *Accounting for uncertainty in DEMs from repeat topographic surveys: improved sediment budgets*, Earth Surface Processes and Landforms, Vol. 35, 2010, pp. 136–156.

[12] **James, M.R.; Robson, S.**: *Straightforward reconstruction of 3D surfaces and topography with a camera: accuracy and geoscience application*, Journal of Geophysical Research: Earth Surface, Vol. 117, 2012.

[13] **Remondino, F.**: *Heritage recording and 3D modeling with photogrammetry and 3D scanning*, Remote Sensing, Vol. 3, No. 6, 2011, pp. 1104–1138.

[14] **Lichti, D.D.**: *Error modelling, calibration and analysis of an AM–CW terrestrial laser scanner system*, ISPRS Journal of Photogrammetry and Remote Sensing, Vol. 61, No. 5, 2007, pp. 307–324.